

Chapter 22

Dynamic Tensile Behavior of a Quenched and Partitioned High Strength Steel Using a Kolsky Bar

Steven Mates and Fadi Abu-Farha

Abstract Dynamic tension tests were performed on a quenched and partitioned high strength steel grade, QP980, using a direct tension Kolsky Bar method. In this method, the steel incident bar consists of a tube section and a solid section of equal impedance mated through a threaded connection. The striker is pneumatically launched within the tube section into an impact cap to create the tensile loading pulse. The transmission bar, which is constructed of aluminum to improve the force measurement sensitivity, is not impedance matched to the incident bar, and as a result the wave analysis technique was modified accordingly. The sample geometry follows ISO 26203-1:2010. Strain-time histories of the specimens obtained by the wave analysis were compared to high speed DIC strain field measurements, and the latter were used to correct the compliance of the test setup. Material tests were performed parallel to, perpendicular to, and at 45° with respect to the rolling direction. Specimens were taken to failure and to several intermediate strain levels by using momentum traps on the incident and transmission bars. Specimen gauge length, gas pressure and striker bar length were changed to achieve different strain rates, covering the range needed for crash simulations. The dynamic behavior of the material is compared to its quasi-static behavior.

Keywords: Kolsky bar • High strain rate • Advanced high strength steels • Automotive light-weighting • High speed digital image correlation

22.1 Introduction

Efforts to improve fleet fuel economy through vehicle weight reduction are currently focused on replacing existing high strength steels with even higher strength grades, known as Advanced High Strength Steels (AHSSs). While some already introduced AHSSs meet the target strength levels (tensile strength higher than 1 GPa), they typically lack the target ductility levels. This not only implies limitations to the sheet formability needed for cold stamping, but also the toughness (energy absorption) needed to meet the desired crashworthiness characteristics. Multi-phase steels containing a retained austenite phase have the potential to provide additional ductility at high strength levels due to the transformation of the retained austenite into martensite in response to plastic deformation. The recently developed class of quenched and partitioned (QP) steels is an example of such multi-phase steels, with a carbon-rich retained austenite phase produced by a partitioning heat treatment, leading to uniform tensile ductility in excess of 10 % at 1 GPa tensile strength [1]. Although not in use in mass-produced automotive components yet, QP steels have great potentials for a wide range of applications in next-generation lightweight vehicles, and they are thus gaining more attention. QP steels have been in commercial production for several years. While their quasi-static deformation behavior has been investigated, efforts characterizing their high rate behavior are very limited. To assess the crashworthiness of these steels, and to supply the data needed for full scale crash simulations using finite element analysis, high strain rate deformation data must be acquired.

In this paper we describe high strain rate tensile measurements of a selected grade of QP steels, the QP980. We use a direct tension Kolsky Bar method in order to facilitate high-speed Digital Image Correlation (DIC) measurements by virtue of unobstructed optical access to the specimen. Tests are performed at different strain rates and different sheet orientations. Moreover, tests are performed to fracture and to intermediate strains (interrupted testing) using momentum trapping to eliminate multiple loadings on the specimen that would otherwise occur due to the reverberation of elastic energy in the Kolsky bar. Data from fracture tests is used to compare the behavior of the material at high rates to that obtained at quasi-

S. Mates (✉)

National Institute of Standards and Technology, 100 Bureau Drive, Gaithersburg, MD, USA

e-mail: steven.mates@nist.gov

F. Abu-Farha

Clemson University—International Center for Automotive Research, Greenville, SC 29607, USA

static conditions. Intermediate strain tests are useful to investigate the microstructural evolution due to the applied dynamic strain, including the change in the retained austenite volume fraction, which will be performed in the future.

22.1.1 Experimental Method

A schematic of the NIST tension Kolsky bar is shown in Fig. 22.1. It utilizes a tubular incident bar concept conceived by Frew and colleagues [2]. This method simplifies the use of pulse-shaping, which is used here to eliminate oscillations in the incident pulse. The incident barrel is constructed of 4340 steel, while the solid portion of the incident bar and the specimen grips are made of hardened maraging steel. The solid portion of the incident bar is 26 mm in diameter and is impedance matched to the barrel. The transmission bar is 20 mm in diameter and made of 7075-T6 aluminum, which provides better force measurement sensitivity compared to steel due to its lower Young's modulus value. Fracture tests are performed using a 1 m long, 20 mm diameter striker bar launched at impact speeds between 6.25 ± 0.05 m/s and 11.4 ± 0.05 m/s. Interrupted strain tests are performed with a 375 mm long, 20 mm diameter striker impacting at 11.6 ± 0.05 m/s. The incident bar momentum trap consists of a 375 mm tube that is impedance matched to the incident barrel. It is placed at a specific distance from the barrel such that it contacts the barrel in time to trap the first pulse that is reflected from the specimen. The transmission bar momentum trap consists of a 375 mm long aluminum tube that is impedance matched to the transmission bar. It is placed concentric with the transmission bar and in contact with a flange fixed to the end of the bar, as shown in Fig. 22.1.

Strain gage data are obtained from 1000- Ω metal foil gages bonded to the incident and transmission bars. Both axial and Poisson strain gages are used on the transmission bar to boost the force sensitivity compared to two axial gages alone. The four gages are arranged in a Wheatstone bridge circuit with a 24 V battery as the excitation source. The sensitivity of the measurement is approximately $81 \mu\epsilon/mV \pm 1 \mu m/m/mV$. The bridge output voltage is recorded at 2 MHz with 14 bit resolution on a 200 mV scale.

Figure 22.2 describes the two sample geometries used for this study. Both specimens follow the recommendations of ISO 26203-1:2010 with regard to the ratio of gage width to gage length (greater than or equal to 2), and to the fillet radius (1.5 mm). Specimens following these geometries were prepared from 1.4 mm thick QP980 sheets using waterjet cutting, followed by precision machining to introduce the grip holes. Two precision alloy steel pins, arranged symmetrically about the load axis, are used on each tab. The pin holes are slightly undersized compared to the pin diameter (5.556 ± 0.008 mm)

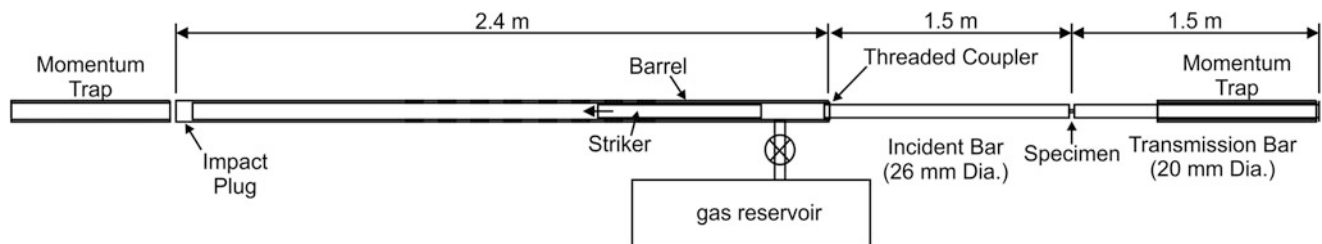


Fig. 22.1 Schematic of NIST direct tension Kolsky bar. Not to scale

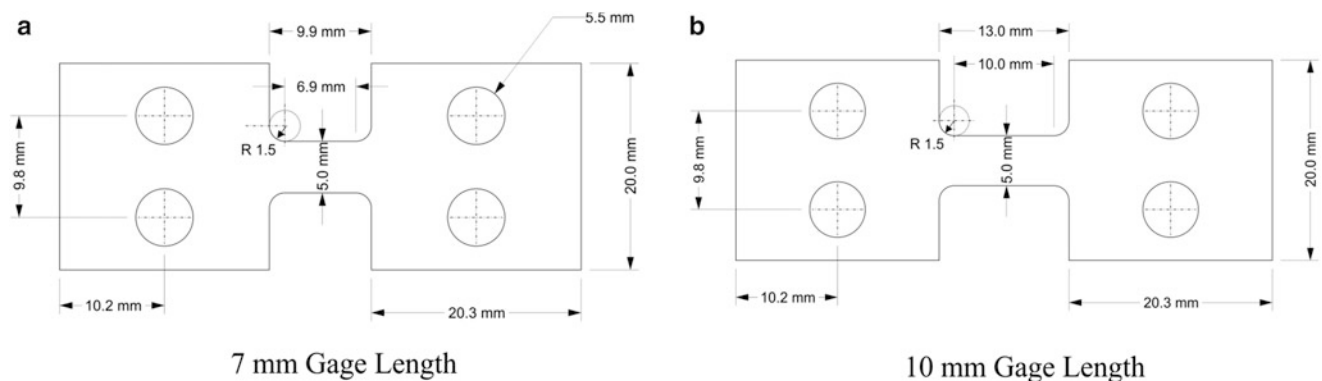


Fig. 22.2 Sample geometries with dimensions in mm, drawn to scale. The specimens are 1.4 mm thick

to promote a small amount of plastic deformation during insertion, which helps prevent slippage during dynamic testing. No adhesive is used. The grips are attached to the bars with ½-20 threads that are treated with Teflon tape to prevent loosening.

Three dimensional digital image correlation (DIC) measurements of the deforming specimen are obtained at 62,500 frames per second with a resolution of 192 by 336 pixels, giving a field of view of approximately 10.3 mm by 18.1 mm, or about 0.05 mm per pixel. Correlation calculations are performed on 21 pixel subsets with a 7 pixel offset. The optical resolving power of the setup, as measured by the 1951 Air Force Target, is 7.13 line pairs per mm. Illumination is provided by a high intensity flash unit operating at 125 W·s with a pulse duration of approximately 1.5 ms. The flash is triggered off the striker bar velocity sensor with a delay programmed to begin the flash at between 5 and 10 frames (80 and 160 μs) prior to the arrival of the tension pulse. The electronic shutter on the cameras is set to 1 μs to eliminate motion blur.

22.1.2 Kolsky Bar Data Analysis

To synchronize the DIC strain-time data with the stress-time data provided by the strain gage output, the DIC strain history, computed by averaging strains over the entire gage area, is first aligned with the strain-time data from the strain gages, which is in turn synchronized with the stress-time data using known wave propagation times between the gages and the sample. The sample strain rate and stress histories are determined using the usual one-dimensional elastic wave analysis with force equilibrium assumed. Using the “3-wave” method for calculating the strain rate, the expression for our Kolsky bar is:

$$\dot{\epsilon} = \frac{[c_i \cdot (\epsilon_i - \epsilon_r) - c_t \cdot \left(\frac{E_i A_i}{E_r A_r}\right) \cdot (\epsilon_i + \epsilon_r)]}{L} \quad (22.1)$$

In (22.1), ϵ is strain, c is elastic wave speed, E is Young’s modulus, A is area and L is length, which can be either instantaneous length for true strain rate, or original length for engineering strain rate. The subscripts i , r and t denote incident, reflected and transmitted, respectively. The expression for stress is:

$$\sigma = \frac{E_t A_t}{A_s} \epsilon_t. \quad (22.2)$$

This expression gives the engineering stress if the original cross-sectional area of the specimen (A_s) is used, or the true stress if the instantaneous area is used.

22.2 Results

Figure 22.3 shows a typical result for a fracture test for a specimen with a 0° orientation with respect to the rolling direction. In this test we use 1 m striker impacting at 9 m/s (+/−0.05 m/s). The top left graph shows the raw strain gage data. In this test there is no momentum trapping, so there are large amplitude reverberations in the strain gage data, as shown in the plot top left. The top right plot shows the strain-time data from the wave analysis method computed using (22.1) and compares the result to the DIC true strain averaged over the entire gage section. As this plot shows, the wave analysis indicates much higher strains in the gage section compared to the DIC average strain. The DIC strain results are considered more accurate since they are derived from localized surface deformation measurements and make no assumption regarding the extent of the deformation zone in the specimen, as the wave analysis method does. The exaggerated strain value provided by the wave analysis is due to deformation occurring outside the nominal gage section (compliance). As such, the wave analysis result is corrected to match the more accurate DIC result using a correction factor, P , that is less than one. In the experiment shown in Fig. 22.3, $P = 0.75$, which is a typical result for these experiments. In general, P may depend on the specimen geometry, the grip technique, and material behavior. The bottom left plot of Fig. 22.3 shows the engineering stress–strain behavior along with the strain-rate versus strain for the experiment. The strain rate increases significantly in the middle of the test, due to localized necking. From this plot, the tensile strength of the steel is about 1120 MPa, and the fracture strain is just over 20 %. However, these results are based on the assumption that the strain distribution within the gage section is uniform until necking begins. The bottom right plot of Fig. 22.3 shows that, while the axial strain distribution is quite symmetric over the gage section, it is never uniform. In this plot the true strain is averaged over cross sections of the specimen along the gage

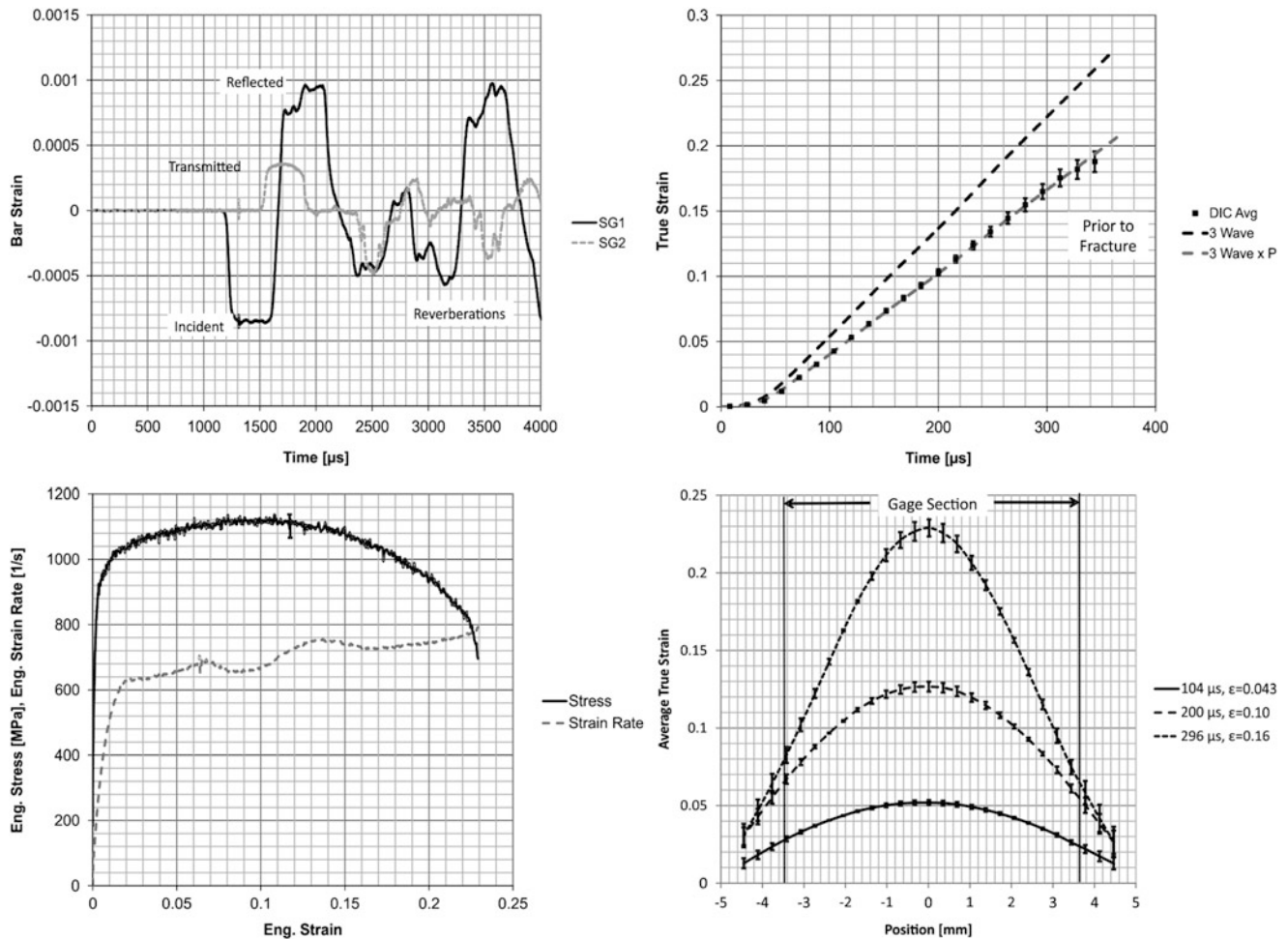


Fig. 22.3 *Top left*: raw strain gage signals from fracture experiment (7 mm gage length, not synchronized with plot *top right*). *Top right*: strain-time from strain gage analysis and average DIC strain over the gage area (DIC error bars are 2 standard deviations of the mean). *Bottom left*: dynamic stress–strain curve and strain rate versus strain. Error bar on stress represents the expanded uncertainty with $k = 2$. *Bottom right*: axial strain distribution along gage length, averaged at each cross section (error bars are one standard deviation)

length. The symmetric profiles indicate good force equilibrium during the test. However, as the plot shows, the distribution is highly peaked. The maximum strain that occurs in the center of the specimen is 20–40 % higher than the average strain, with the proportion increasing with average strain. We believe this is the underlying cause of the observation that fracture always occurred in the center of the specimen in our tests. The highly peaked strain distributions seen here agree generally with recently published numerical simulations of dynamic tension tests with similar gage-length to gage-width ratios [3]. Because the strains are so non-uniform over the gage length, the engineering stress–strain curve shown in Fig. 22.3 is not a very meaningful representation of the real material behavior. The data remain useful, though, for examining the relative effects of strain rate and rolling direction. Going forward, DIC measurements must be better leveraged to determine the dynamic tensile behavior of this material up to and beyond necking, using either a Bridgman-like correction technique [4] or finite element modeling and inverse methods.

Figure 22.4 describes an interrupted strain experiment for a 0° orientation specimen using a 375 mm striker impacting at 11.6 m/s (± 0.05 m/s). In this experiment the momentum traps are engaged, so the amplitude of the reverberations is much smaller compared to the results shown in Fig 22.3. The top right plot shows the DIC average strain versus time for this test along with the compensated strain result from the wave analysis (here $P = 0.77$). The specimen experiences just over 10 % engineering strain and has yet to begin localized necking. As with the fracture test presented in Fig. 22.3, the present test has a non-uniform, yet highly symmetric, axial strain distribution. The DIC measurements capture the elastic recovery that occurs as the load is removed, amounting to 0.65 %. This value corresponds well to the expected amount of elastic strain in the specimen at the peak load level, considering a nominal Young’s modulus of 200 GPa for this material. The elastic

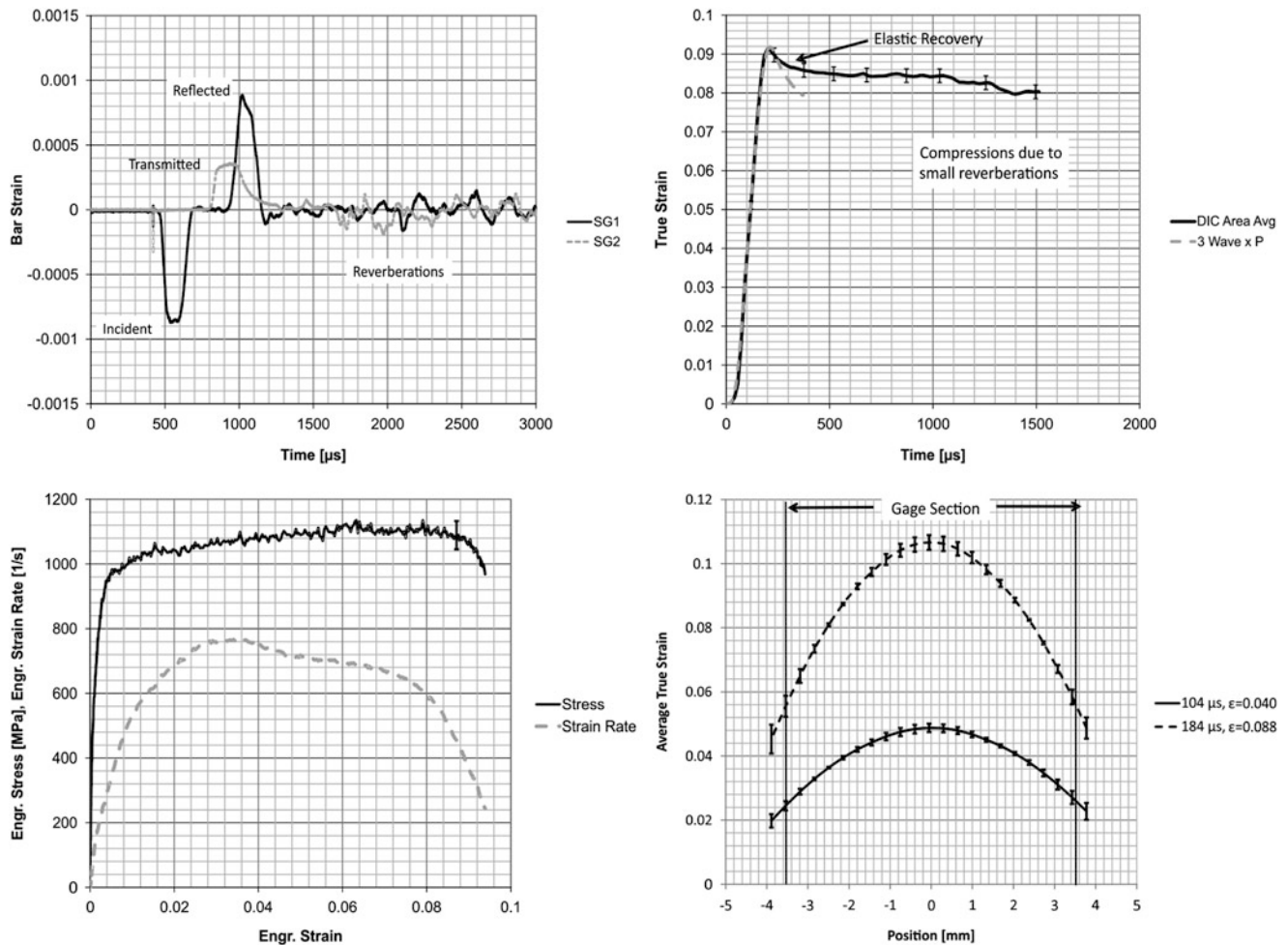


Fig. 22.4 *Top left*: raw strain gage signals from a recovery experiment (7 mm gage length, not synchronized with plot *Top right*). *Top right*: strain-time from strain gage analysis and average DIC strain over the gage area (DIC data error bars are twice the standard deviation of the mean). *Bottom left*: dynamic stress–strain curve and strain rate versus strain. Error bar on stress represents the expanded uncertainty with $k = 2$. *Bottom right*: axial strain distribution along gage length, averaged at each cross section (error bars are one standard deviation)

recovery occurs within 300 μs of the peak load, after which the average strain settles to a constant level. Then, at 1100 μs and again at 1400 μs , the specimen experiences a small compressive strain (about 0.25 % in aggregate) due to reverberations in the bar that remain despite the momentum trapping.

Figure 22.5 shows three experiments for the 7 mm gage length and the 0° orientation where the striker velocity is increased to examine the effect of strain rate on the plastic behavior. As the plot shows, there is little difference in the curves until the peak stress. At the lowest dynamic strain rate the specimen did not fracture, so the drop off in stress occurs because the load pulse comes to an end. As a result, no ductility information is available at this strain rate. The highest strain rate shows slightly less ductility at fracture compared to the intermediate strain rate, although the difference is small. Compared to the quasi-static strength (measured following ASTM E8), QP980 shows measureable strain rate hardening, which generally agrees with the trends observed in other multi-phase steels with retained austenite in the microstructure, such as TRIP steels [5]. It is note mentioning here that the stress–strain curves for both the quasi-static and high rate cases show similar hardening behaviors with comparable uniform strains ($\sim 12\%$); the high rate curves stretch further in the non-uniform deformation portion simply due to the smaller specimens with lower gage width-to-length ratio. Figure 22.6 examines the effect of orientation with respect to the rolling direction for this sheet steel. As the figure shows, there is very little influence of rolling direction on the dynamic fracture behavior. Thus, whatever preferred texture is introduced into the grain structure via the rolling process has little influence over the dynamic strength and ductility of this particular high strength steel.

Fig. 22.5 The effect of strain rate on QP980, using 7 mm gauge length specimens. Error bar represents 2k expanded uncertainty and is typical for all tests

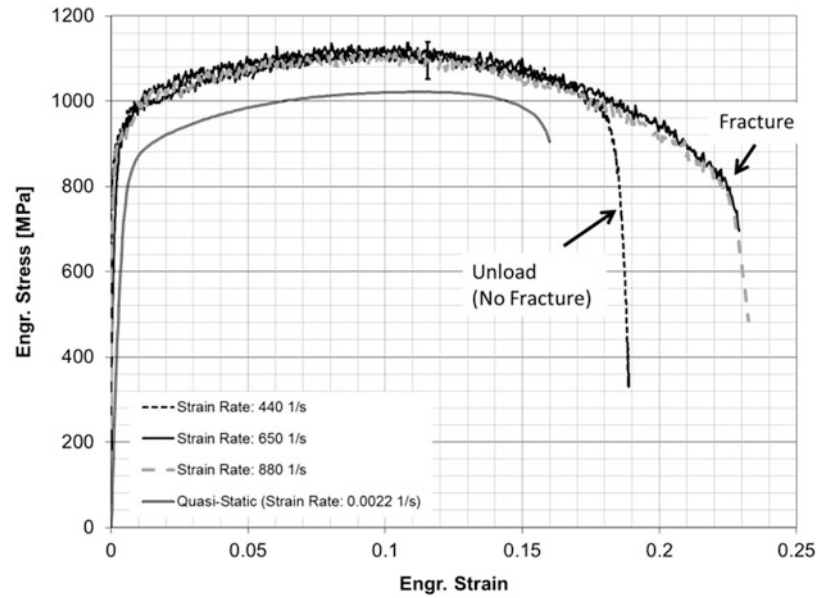
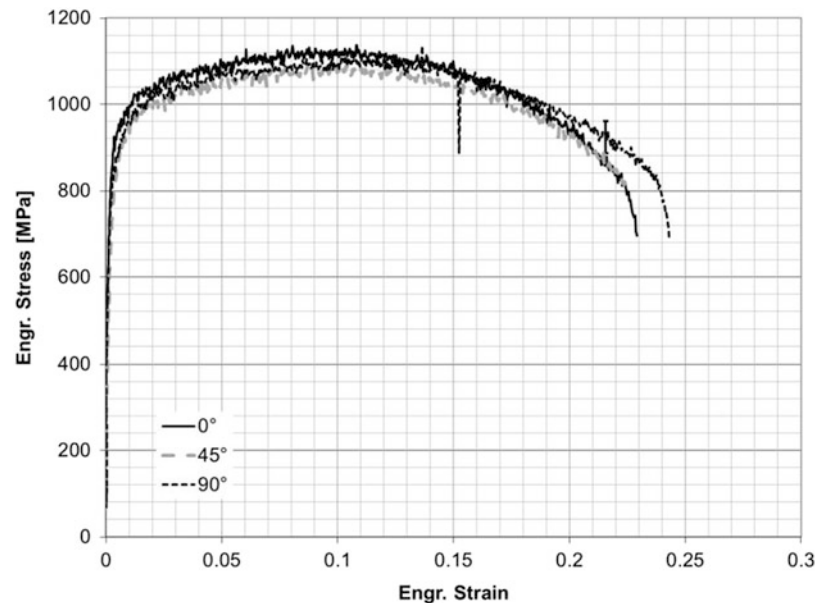


Fig. 22.6 The effect of orientation with respect to the rolling direction on QP980 fracture behavior. Tests are conducted with 7 mm gauge length specimens at a strain rate of 650 s^{-1} . Error bar represents the expanded uncertainty with $k = 2$



22.3 Conclusions

High strain rate tension tests are conducted on a quenched and partitioned high strength steel grade (QP980) to compare with the material behavior at quasi-static rates, for crashworthiness assessment. High speed 3D DIC is used to measure the strain distribution of the specimens during deformation. Interrupted strain tests are performed to several intermediate strains to investigate the microstructural evolution resulting from large strain dynamic tensile deformation. The DIC measurements showed that significantly less strain occurs in the gage section compared to the strain indicated by the strain gage analysis method, which assumes all displacement that occurs between the grips converts to strain within the gage section. This turned out to be an invalid assumption in these experiments. The DIC measurements were also able to capture the magnitude of elastic recovery that occurs in the specimens during interrupted-strain testing. Finally, the DIC measurements showed that while axial strain distributions are highly symmetric they are also very non-uniform. Finally, the orientation of the specimen with respect to the rolling direction nor a factor of two increase in strain rate (from 440 1/s to 880 1/s) had much influence on

the mechanical behavior of this material. The results obtained here for the QP980 will be used for comparison with other grades of conventional AHSSs. Moreover, they will serve as the baseline for comparisons with future generations of AHSSs that are currently under development.

Acknowledgment/Disclaimer This material is based upon work supported by the Department of Energy under Cooperative Agreement Number DE-EE0005976, with United States Automotive Materials Partnership LLC (USAMP). This support is greatly appreciated.

This report was prepared as an account of work sponsored by an agency of the United States Government. Neither the United States Government nor any agency thereof, nor any of their employees, makes any warranty, express or implied, or assumes any legal liability or responsibility for the accuracy, completeness, or usefulness of any information, apparatus, product, or process disclosed, or represents that its use would not infringe privately owned rights. Reference herein to any specific commercial product, process, or service by trade name, trademark, manufacturer, or otherwise does not necessarily constitute or imply its endorsement, recommendation, or favoring by the United States Government or any agency thereof. The views and opinions of authors expressed herein do not necessarily state or reflect those of the United States Government or any agency thereof.

References

1. Speer, J., Assuncao, F., Matlock, D., Edmonds, D.: The “quenching and partitioning” process: background and recent progress. *Mater. Res.* **8**, 417–423 (2005)
2. Guzman, O., Frew, D.J., Chen, W.: A Kolsky tension bar technique using a hollow incident tube. *Meas. Sci. Technol.* **22**, 9 (2011)
3. Rotbaum, Y., Rittel, D.: Is there an optimal gauge length for dynamic tensile specimens? *Exp. Mech.* **54**(7), 1205–1214 (2008)
4. Bridgman, P.W.: The stress distribution at the neck of a tension specimen. *Trans. ASM* **32**, 553 (1944)
5. Huh, H., Kim, S., Song, J., Lim, J.: Dynamic tensile characteristics of TRIP-type and DP-type steel sheets for an auto-body. *Int. J. Mech. Sci.* **50**, 918–931 (2008)